Scientific Journals

ISSN 2049-954X

Chemistry Journal

Research Paper

Electrical Analysis of Bis (2-Amino-4-Methylpyridinium) Tetrachloridozincate Compound Grown by Chemical Bath Deposition at Ambient Temperature and Pressure Conditions

Cliff Orori Mosiori[1]* and John Maera[2]

[1]*Department of Physics, Kenyatta University, P. O Box 43844-00100, Kenya*
[2]*Department of Physics, Maasai Mara University, P.O. Box 430-20050 Narok, Kenya*
**E-Mail: cliffmosiori@gmail.com*

Abstract

In this paper, a study was carried out and we now report the measurement of impedance spectroscopy for the bis(2-amino-4-methylpyridinium) tetrachloridozincate (II) compound in the frequency range 209 Hz-5 MHz with the temperature ranging from 308 up to 368 K. The results are represented in impedance plots which have shown semicircle arcs at different temperatures and an electrical equivalent circuit has been proposed to explain the impedance results. Detailed analysis of the impedance spectrum suggests that the electrical properties of the material are strongly temperature dependent. The frequency-dependent conductivity data were fitted in the Jonscher's law: $\sigma_{ac}(\omega) = \sigma_{dc} + A\omega^n$. The conductivity follows the Arrhenius relation. Thus the conduction in the material is probably due to a hopping or a small polar on tunnelling process. It was concluded that the temperature dependence of conductivity was analyzed using the Arrhenius approach. Finally the AC conductivity of $[C_6H_9N_2]_2ZnCl_4$ material was studied as a function of temperature (308-368 K) and frequency ranges (209 Hz to 5 MHz), respectively. The AC conductivity has shown a variation with frequency and was found to obey Jonscher's law: $\sigma_{ac} = \sigma_{dc} + A\omega^n$ at different temperatures. The temperature dependence of the Jonscher's exponent has revealed that the conduction inside the studied material is insured by the Non-overlapping Small Polaron Tunnelling (NSPT) model.

Keywords: *Impedance Spectroscopy, Equivalent Circuit, Electrical Properties, Conductivity*

1. Introduction

Considerable interest has been devoted to compounds of the general formula A_2MX_4 where A is an organic cation, M a divalent metal (Cu, Sb, Cd, Hg.…) and X a halogen (Cl, Br) (Masmoudi et al, 2012; Karoui et al, 2013 and Weslati et al, 2014). The hybrid organic-inorganic materials have generated a lot of interest from the technological and scientific points of view that may combine desirable physical properties characteristic (Chaabane et al, 2008; Khelifi et al, 2010 and Elwej et al, 2014). Indeed, the synthesis of low-dimensional mixed inorganic-organic materials enables both inorganic and organic components at the molecular level to be optimized and thus to exhibit specific properties such as optical, electronic and thermal (Medycki et al, 2003; Wojtas et al, 2008 and Genovese & Lian, 2015) and structural phase transitions (Hannachi et al, 2010; Ben Bachir et al, 2014; Weslati et al, 2014 and Ben Mohamed et al 2015). In recent years, the impedance spectroscopy is considered as one of important experimental techniques to analyze the dynamics of ionic mobility in solids (Ahmad & Yamada, 2002; Padmasree & Kanchan, 2005; Louati et al, 2009; Jarboui et al, 2010; Louati & Guidara, 2011 and Mahamoud et al, 2011).

In this paper we report the synthesis of bis (2-amino-4-methylpyridinium) tetrachloridozincate (II) and characterised by X-ray powder diffraction patterns, the differential

scanning calorimetry and the results of the impedance spectroscopy are discussed, the temperature and frequency dependence of the electrical conductivity and the modulus properties of the $[C_6H_9N_2]_2ZnCl_4$ compound.

2. Materials and Methods

The $[C_6H_9N_2]_2ZnCl_4$ sample was prepared by mixing $ZnCl_2$ (purity 98%; Fluka), dissolved in hydrochloric acid solution (1M) and the organic compound bis (2-amino-4-methylpyridinium) (purity 99%; Fluka), in molar ratio 1:2.

Schematically the reaction proposed in order to justify the obtaining bis (2-amino-4-methylpyridinium) tetrachloridezincate (II) sample is shown in the following equation:

$$2(C_6H_8N_2) + ZnCl_2 \xrightarrow{2HCl} [C_6H_9N_2]_2ZnCl_4 \ldots\ldots\ldots\ldots 1$$

After one week, crystalline samples were obtained by slow evaporation at room temperature. The sample was characterised by the X-ray powder pattern using a Phillips powder diffractometer PW with CuKα radiation (λ= 1.5405) in a wide range of Bragg angles ($10° \leq 2\theta \leq 40°$). Differential scanning calorimetric analysis was performed using a DSC NETZSCH 204 between 25-300 °C at the heating rate of 5 °C/min. The electrical measurements were performed using two electrode configurations. The powder was pressed into a pellet of 8 mm diameter and 1.2 mm thickness. The AC conductivity was measured using a TEGAM 3550 impedance analyser, automatic bridge monitored by a microcomputer between 308-368 K temperature; measuring real and imaginary parts of the sample impedance in the frequency range 209 Hz-5 MHz as shown in the Table 1.

Table 1. Real and Imaginary Parts of the Sample Impedance in the Frequency Range 209 Hz–5 MHz

T (K)	R (10^7)	Q_1 (10^{-11})	α_1	Q_2 (10^{-7})	α_2
308	1.24	3.81	0.812	-	-
313	1.08	4.26	0.801	-	-
318	0.75	4.27	0.812	-	-
323	0.45	4.58	0.814	-	-
328	0.21	4.40	0.844	-	-
333	0.11	5.56	0.817	-	-
338	0.06	4.87	0.839	1.23	0.874
343	0.042	4.34	0.852	9.63	0.584
348	0.032	3.77	0.867	15.2	0.522
353	0.021	2.60	0.905	28.19	0.437
358	0.015	2.33	0.912	32.91	0.439
363	0.0109	1.93	0.932	39.72	0.439
368	0.008	1.66	0.947	48.06	0.432

T= Temperature; R= Reflectance; Q =Quality Factor; α = Absorption

3. Results and Discussion

3.1. X-Ray Powder Analysis

The room temperature X-Ray diffraction pattern of the bis (2-amino-4-methylpyridinium) tetrachloridozincate (II) is shown in Figure 1. The sample crystallizes in the triclinic, space group $P\bar{1}$ with the unit cell parameters a = 7.471 (2) Å, b = 8.467 (1) Å, c = 15.379 (5) Å, α = 95.09 (2)°, β = 91,12 (2)° and γ = 70.05 (2)°. From these, it is found that $[C_6H_9N_2]_2ZnCl_4$ is in a good agreement with the literature values (Gharbia et al, 2008).

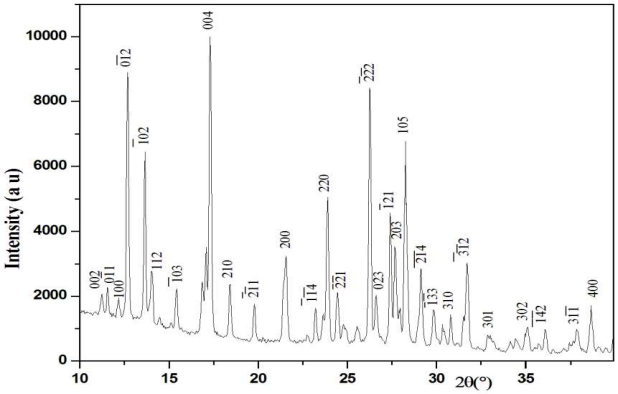

Figure 1. X-Ray Diffraction Pattern of the bis (2-amino-4-methylpyridinium) tetrachloridozincate (II)

3.2. DSC Analysis

Results of differential scanning calorimetry measurements, recorded in the temperature range 25-300 K are presented in the thermogram. It shows the presence of an endothermic peak located at 159.53 ^oC corresponding to the fusion of the compound $[C_6H_9N_2]_2ZnCl_4$.

3.3. Impedance Analysis

The impedance diagrams (Figure 2) for $[C_6H_9N_2]_2ZnCl_4$ sample are taken in the temperature range 308-368 K. The equivalent circuit allows the establishment of correlations between electrochemical parameters and characteristic impedance elements. In the temperature range 308-333 K, the equivalent circuit consists of a resistance R1 (bulk resistance) and CPE1 (capacity of the fractal interface CPE1) element (Figure 3). The CPE element accounts for the non-ideal electrode geometry (Milankovic et al, 2005; Hannachi et al, 2010 and Makram et al, 2010).

The impedance of CPE (Behera et al, 2007 and Rao et al, 2008) is:

$$ZCPE = 1/ (Q(j\omega)^{\alpha}) \ldots\ldots\ldots\ldots 2$$

α is related to the deviation from the vertical of the line in

the -Z″ versus Z′ plot. A = 1 indicates a perfect capacitance, if α = 0; CPE behaves as a pure resistor, while if α = -1; CPE behaves like an inductor, thus α values directly reflect on the roughness of the electrode used. In the rest of the temperature range (T ≥ 338 K), the above circuit is inadequate; the measured values disagree with the simulated one. We observe a little tail after the semicircles in the impedance spectra. The straight line after the semicircle can be explained with CPE2 corresponding to the double layer capacity of an inhomogeneous electrode surface.

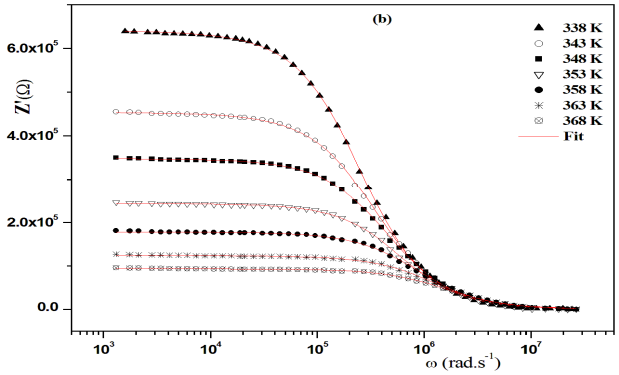

Figure 2. Impedance Diagrams Curves Taken in the Temperature Ranges Shown

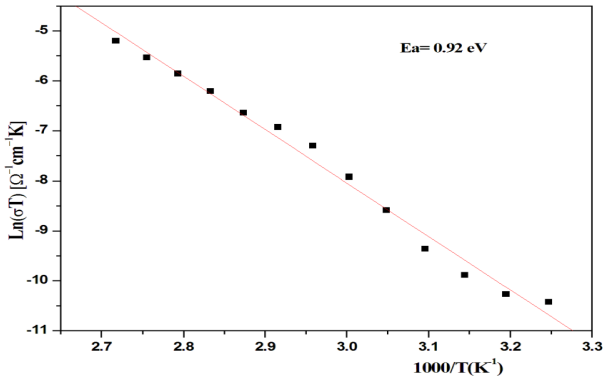

Figure 3. Variation of Real Part of the Impedance at Different Lower Temperatures in the Low-Frequency Region

The expression of real Z' and imaginary -Z'' components of impedance related to the equivalent circuits are:

- For the first circuit (R1 // CPE1):

$$Z' = \frac{R_p^2 Q\omega^{\alpha}\cos(\alpha\pi/2) + R_p}{(1+R_p Q\omega^{\alpha}\cos(\alpha\pi/2))^2 + (R_p Q\omega^{\alpha}\sin(\alpha\pi/2))^2} \quad \text{……...…….3}$$

$$-Z'' = \frac{R_p^2 Q\omega^{\alpha}\sin(\alpha\pi/2)}{(1+R_p Q\omega^{\alpha}\cos(\alpha\pi/2))^2 + (R_p Q\omega^{\alpha}\sin(\alpha\pi/2))^2} \quad \text{……...……4}$$

- For the second circuit (R1 // CPE1 + CPE2):

$$Z' = \frac{R_p^2 Q_1\omega^{\alpha_1}\cos(\alpha_1\pi/2) + R_p}{(1+R_p Q_1\omega^{\alpha_1}\cos(\alpha_1\pi/2))^2 + (R_p Q_1\omega^{\alpha_1}\sin(\alpha_1\pi/2))^2} + \frac{\cos(\alpha_2\pi/2)}{Q_2\omega^{\alpha_2}} \quad \text{…..……5}$$

$$-Z'' = \frac{R_p^2 Q_1\omega^{\alpha_1}\sin(\alpha_1\pi/2)}{(1+R_p Q_1\omega^{\alpha_1}\cos(\alpha_1\pi/2))^2 + (R_p Q_1\omega^{\alpha_1}\sin(\alpha_1\pi/2))^2} + \frac{\sin(\alpha_2\pi/2)}{Q_2\omega^{\alpha_2}} \quad \text{..……6}$$

The resistance R_p, Q and α have been simulated using a mean square method which consists in minimizing the difference between the experimental and calculating data. The values of the equivalent circuit elements have been evaluated and listed in Table 1. Figure 3 shows the variation of real part of the impedance at different temperatures. The impedance value is typically higher at lower temperatures in the low-frequency region, and then it decreases gradually with increasing frequency.

Figure 3 shows the variation of the imaginary part of impedance with frequency for some representative temperatureies. The spectra are characterised by the appearance of peaks, which shift to higher frequencies with increasing temperature. Such behaviour indicates the presence of relaxation in the system. The good conformity of calculated lines with the experimental data indicates that the suggested equivalent circuit describes the pellet–electrolyte interface reasonably well.

3.4. Conductivity Study

3.4.1. DC Conductivity

The values of bulk resistance, R, for the single semicircle together with electrode dimensions (S is the area of the sample and e is the sample thickness) are used to determine the DC conductivity. The direct current conductivity (σ_{dc}) has been calculated at each temperature by means of the relation:

$$\sigma = e/R.S \quad \text{……...…7}$$

The activation energies Ea of the dc conduction are obtainned using the Arrhenius equation:

$$\sigma T = A \exp(-Ea/k_B T) \quad \text{……..8}$$

Where:

A: The pre-exponential factor
Ea: The activation energy
T: The absolute temperature
k_B: The Boltzmann constant

Following the Arrhenius law, the obtained activation energy is about Ea=0.92 (1) eV.

3.4.2. AC Conductivity

The frequency variation of the AC conductivity, $\sigma_{ac}(\omega)$, at various temperature. The σ_{ac} increases with increasing fre-

quency, which is a characteristic of ω^n. The conductivity results are fitted by the following equation referred to as Jonscher's power law (Chouaib et al, 2011):

$$\sigma_{ac} = \sigma_{dc} + A\omega^n \quad \text{.....9}$$

Where:

σ_{dc}*: The D.C. conductivity*
A: The temperature-dependent parameter that determines the strength of polaribility
n: Dimensional frequency exponent parameter in the range of $0 \leq n \leq 1$

n is the dimensional frequency exponent parameter (Figure 4) in the range of $0 \leq n \leq 1$ (Lee et al, 1991 and Elwej et al, 2015) representing a degree of interaction between mobile ions with the lattices around them: the 'universal' dynamic pattern of the AC electrical behaviour of conducting solids and liquids as proposed by Jonscher. It is obvious that the experimental and fitted data are very close. Using Eq. 9 n increases according to the temperature and varies between $0.54 \leq n \leq 0.86$, which indicates that the electrical conduction is provided by the non-overlapping small Polaron Tunnelling (NSPT) model (Mansour et al, 2010 and Hamdi et al, 2015).

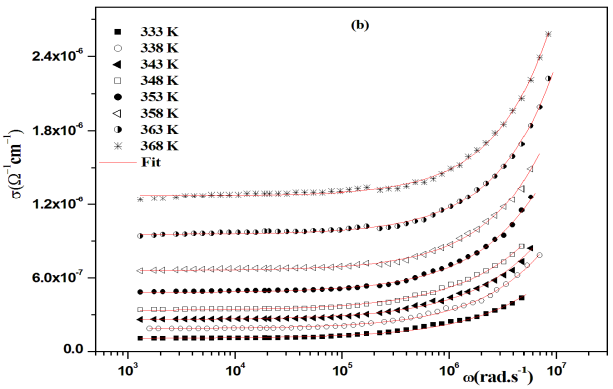

Figure 4. AC Electrical Behaviour of Conducting Solids and Liquids as Dimensional Frequency Exponent Parameter

3.5. Dielectric Studies

The study of the dielectric properties is an important source of valuable information about conduction processes since we can determine the origin of the dielectric losses, the electrical relaxation time and its activation energy (Hannachi et al, 2010).

The dielectric relaxation is described by a non-Debye model which gives the frequency-dependent complex permittivity in the form (Rhouma et al, 2012):

$$\varepsilon^*(\omega) = \varepsilon_\infty + \frac{\varepsilon_s - \varepsilon_\infty}{1 + (\frac{i\omega}{\omega_1})^{1-\alpha}} + \frac{\sigma_0}{i\varepsilon_0\omega} \quad \text{.....10}$$

The imaginary part of the complex permittivity is:

$$\varepsilon''(\omega) = \frac{(\varepsilon_s - \varepsilon_\infty)(\frac{\omega}{\omega_1})^{1-\alpha}\sin(\frac{(1-\alpha)\pi}{2})}{1 + 2(\frac{\omega}{\omega_1})^{1-\alpha}\cos(\frac{(1-\alpha)\pi}{2}) + (\frac{\omega}{\omega_1})^{2(1-\alpha)}} + \frac{\sigma_0}{\varepsilon_0\omega} \quad \text{.....11}$$

Where:

ε_s*: The static permittivity*
ε_∞*: The permittivity at "infinitely" high frequency*
σ_0*: The specific conductivity*
ε_0*: The dielectric permittivity of vacuum*
α*: The tilting angle* ($\alpha\varpi/2$) *of the circular arc from the real axis in the complex permittivity plane*
ω*: The angular frequency*

According to Nithya et al (2011), the dielectric constant increases with the increase in temperature because of the total polarization that arises from the dipole orientation and the trapped charge carriers. The dielectric dispersion rises drastically toward low frequencies and decays at higher frequencies. The dielectric profile plot is higher at low frequencies possibly because of the different types of polarization effects. These effects may be caused by more of the contribution polarization factors (atomic, electronic, interfacial factors). Higher dielectric constants at low frequencies depend on ionic vibration or movement and space charge effects. Thus, the higher value of e at the low frequency region is most probably due to electrode polarization and space charge effects confirming the non-Debye dependence (Kumar et al, 2010 and Kumar & Srivastava, 2014). This dispersion reflects the existence of space charge polarization where enough time is provided for the charges to build up at the interface before the applied field changes direction. Best fits using the function Eq. 11 provides a suitable fitting of the curves resulting from the experimental data in Figure 5.

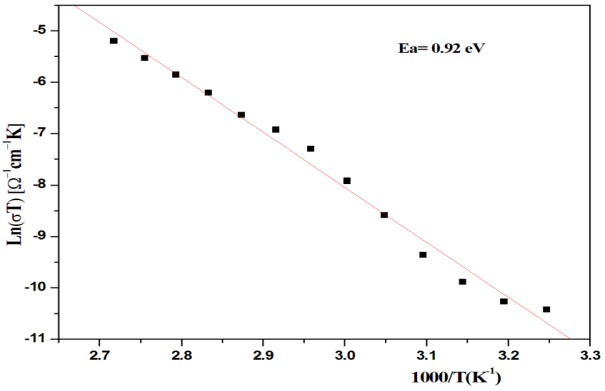

Figure 5. Caption

3.6. Complex Modulus Analysis

The electric modulus (M^*) is calculated from the following equation:

$$M^* = j\Delta C_0 Z^* = M' + j\,M'' \quad \text{.....12}$$

Where:

M′ and M″: Real and imaginary part of electric modulus respectively
C_0: The vacuum capacitance of the measuring cell

Together with:

$M' = \omega C_0 Z'$ and $M'' = \omega C_0 Z''$……...13

Where:

$C_0 = \Delta_0 S / e$
Δ_0: The permittivity of vacuum
S: The surface of the sample
E: The sample thickness
$\Delta = 2\Delta f$

Figure 6 shows the frequency dependence of the real and imaginary part of the electrical modulus (M′ and M″) of $[C_6H_9N_2]_2ZnCl_4$ compound at different temperatures. The plot of imaginary part of M shows a slightly asymmetric peak at each temperature. The peak shifts toward higher angular frequencies (10^7) with the increase in temperature, indicating correlation between the motions of mobile ion charges. The asymmetry in peak broadening shows the spread of relaxation times with different time constants (Masmoudi et al, 2012). The frequency of the modulus maximum shifts to higher frequency side with the increase in temperature. The peaks existing at low frequency suggests that the ions can move over long distances, whereas high-frequency peaks suggest the confinement of ions in their potential well. The nature of the modulus spectrum confirms the existence of hopping mechanism in the electrical conduction of the material (Prabakar et al, 2003).

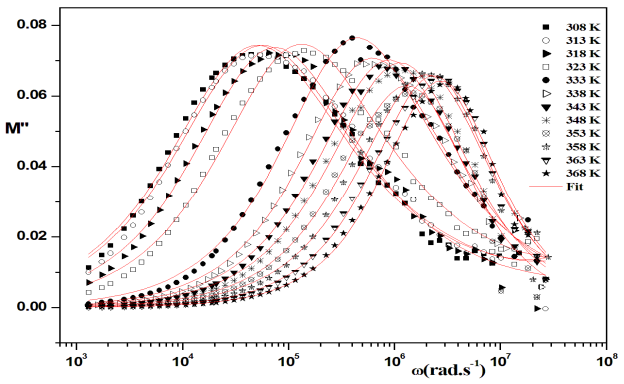

Figure 6. Imaginary Part of Electric Modulus

The variations of the imaginary part of the modulus pass through a maximum at $\omega\tau = 1$, where τ is the average electric field relaxation time. The region to the left of the peak is where the ions are mobile over long distances; the region to the right is where the ions are spatially confined to their potential wells. The frequency range where the peak occurs is indicative of the transition from short-range to long-range mobility and at temperature (333 K); there is a change from one circuit to another. The plot of the relaxation time (Figure 6) may be described by Arrhenius law:

$\tau = \tau_0 \exp(Ea/kT)$……14

Where:

τ_0: The characteristic relaxation time
Ea: The energy, (Ea=0.85 eV)
K: The Boltzmann constant

4. Conclusion

This study of the diffraction of X-rays on powder showed that bis(2-amino-4-methylpyridinium) tetrachloridozincate (II) crystallizes in the triclinic system has a unit cell of dimensional parameters in which a = 7.471 (2) Å, b = 8.467 (1) Å, c = 15.379 (5) Å, α = 95.09 (2)°, β = 91,12 (2)° and γ = 70.05 (2)°. It can also be noted here that similar X-ray diffraction data collection and interpretation was also described by Gharbia et al (2008). The differential calorimetric analysis studies also showed that the presence of only one endothermic peak located at 159.53 °C which corresponds to the fusion of material. On the other hand, the analysis of the frequency dispersion of the real imaginary components of the complex impedance allowed us to determine two equivalent electrical circuits for this material. The temperature dependence of conductivity was analyzed using the Arrhenius approach. Finally the AC conductivity of $[C_6H_9N_2]_2ZnCl_4$ material was studied as a function of temperature and frequency ranges (308-368 K) and (209 Hz to 5 MHz), respectively. The AC conductivity has shown a variation with frequency and was found to obey Jonscher's law: $\sigma_{ac} = \sigma_{dc} + A\omega^n$ at different temperatures. The temperature dependence of the Jonscher's exponent has revealed that the conduction inside the studied material is insured by the non-overlapping small Polaron Tunnelling (NSPT) model.

Acknowledgement

We acknowledge the financial support and cooperation given by the departments of Physic at Kenyatta and Maasai Mara University. We also acknowledge the University of Nairobi, Department of Material Science, Chiromo Campus, for allowing us use their instruments to measure and analyse the work reported here.

References

Ahmad, M., and Yamada, T. (2002) Frequency dependent conductivity and dielectric studies on $RbSn_2F_5$. **Solid State Communications**, 123(5), pp. 185-189.

Behera, B., Nayak, P., and Choudhary, R.N.P. (2007) Impedance spectroscopy study of $NaBa_2V_5O_{15}$ ceramic. **J. Alloys Compd.**, 436, p. 226.

Ben Bachir, M., Karoui, K., Tabellout, M., Guidara, K., and Ben Rhaiem, A. (2014) Electric and dielectric studies of the $[N(CH_3)_3H]_2CuCl_4$ compound at low temperature. **J. Alloys Compd.**, 588, p. 551.

Ben Mohamed, C., Karoui, K., Jomni, F., Guidara, K., and Ben Rhaiem, A. (2015) Electrical properties and conduction mechanism of $[C_2H_5NH_3]_2CuCl_4$ compound. **J. Mol. Struct.**, 1082, p. 38.

Chaabane, I., Hlel, F., and Guidara, K. (2008) Electrical study by impedance spectroscopy of the new compound $[C_{12}H_{17}N_2]_2CdCl_4$. **Journal of Alloys and Compounds**, 461, p. 495.

Chouaib, S., Rhaiem, A., and Guidara, K. (2011) Dielectric relaxation and ionic conductivity studies of $Na_2ZnP_2O_7$. **Bull. Mater. Sci.**, 34, p. 915.

Elwej, R., Hamdi, M., Hannachi, N., and Hlel, F. (2014) Synthesis, structural characterization and dielectric properties of $(C_6H_9N_2)_2(Hg_{0.75}Cd_{0.25})Cl_4$ compound. **Spectrochim. Acta, Part A: Mol. Biomol. Spectrosc.**, 121, p. 632.

Elwej, R., Hamdi, M., Hannachi, N., and Hlel, F. (2015) Temperature- and frequency-dependent dielectric properties of organic–inorganic hybrid compound: $(C_6H_9N_2)_2(Hg_{0.75}Cd_{0.25})Cl_4$. **Mater. Res. Bull.**, 62, p. 42.

Genovese, M., and Lian, K. (2015) Polyoxometalate modified inorganic-organic nanocomposite materials for energy storage applications: A review. **Curr. Opin. Solid State Mater. Sci.**, 19, p. 126.

Gharbia, I., Kefi, R., Nasr, B., and Durif, A. (2008) Structure and characterization of a new inorganic-organic hybrid complex of Zn(II) with 2-amino-4-methylpyridine. **Revue Roumaine of Chimie**, 53, p. 169.

Hamdi, M., Louati, B., Lafond, A., Guillot-Deudon, C., Chrif, B., Khirouni, K., Gargouri, M., Jobic, S., and Hlel, F. (2015) Structural and electrical properties of $Cu_2Zn(Sn_{1-x}Si_x)S_4$ (x =0, x = 0.5) materials for photovoltaic applications. **J. Alloys Compd.**, 620, p. 434.

Hannachi, N., Chaabane, I., Guidara, K., Bulou, A., and Hlel, F. (2010) AC electrical properties and dielectric relaxation of $[N(C_3H_7)_4]_2Cd_2Cl_6$, single crystal. **Mater. Sci. Eng., B**, 172, p. 24.

Hannachi, N., Guidara, K., Bulou, A., and Hlel, F. (2010) Structural characterization and AC conductivity of bis tetrapropylammonium hexachlorado-dicadmate, $[N(C_3H_7)_4]_2Cd_2Cl_6$. **Mater. Res. Bull.**, 45, p. 1754.

Jarboui, A., Ben Rhaeim, A., Hlel, F., Guidara, K., and Gargouri, M. (2010) NMR study and electrical properties investigation of $Zn_2P_2O_7$. **Ionics**, 16, p. 67.

Karoui, K., Ben Rhaiem, A., Jomni, F., Moneger, J.L., Bulou, A., and Guidara, K. (2013) Characterization of phase transitions of $[N(CH_3)_4]_2ZnCl_2Br_2$ mixed crystals. **J. Mol. Struct.**, 1048, p. 287.

Khelifi, M., Mkaouar, I., Hlel, F., Salah, A., and Ben Zouari, R. (2010) Crystal structure and electrical properties study of 4-amino pyridinium chloride bismuthate (III) $(C_5N_2H_7)_4.HBi_2Cl_{11}$. **Ionics**, 16, p. 709.

Kumar, D., Arun, S., Selvasekarapandian, S., Nithya, H., Sakunthala, A., and Hema, M. (2010) Dielectric, modulus and impedance analysis of LaF_3 nanoparticles. **Physica B: Condens. Matter**, 405, p. 3803.

Kumar, M., and Srivastava, N. (2014) Investigation of electrical and dielectric properties of NaI doped synthesized systems. **J. Non-Cryst. Solids**, 389, p. 28.

Lee, W.K., Liu, J.F., and Nowick, A.S. (1991) Limiting behavior of ac conductivity in ionically conducting crystals and glasses: A new universality. **Phys. Rev. Lett.**, 67, p. 1559.

Louati, B., and Guidara, K. (2011) Dielectric relaxation and ionic conductivity studies of $LiCaPO_4$. **Ionics**, 17, p. 633.

Louati, B., Guidara, K., and Gargouri, M. (2009) Dielectric and ac ionic conductivity investigations in the monetite. **J. Alloys Compd.**, 472, p. 347.

Mahamoud, H., Louati, B., Hlel, F., and Guidara, K. (2011) Conductivity and dielectric studies on $(Na_{0\cdot4}Ag_{0\cdot6})_2PbP_2O_7$ compound. **Bull. Mater. Sci.**, 34, p. 1069.

Makram, M., Mahmoud, H., Louati, B., Hlel, F., and Guidara, K. (2010) AC electrical properties study and equivalent circuit of a monovalent-mixed pyrophosphate. **Ionics**, 16, p. 655.

Mansour, Sh.A., Yahia, I.S., and Sakr, G.B. (2010) Electrical conductivity and dielectric relaxation behavior of fluoresce in sodium salt (FSS). **Solid State Commun.**, 150, p. 1386.

Masmoudi, W., Kamoun, S., and Gargouri, M. (2012) AC conductivity and dielectric studies of $(C_5H_{10}N)_2BiCl_5$ compound. **Ionics**, 18, p. 117.

Masmoudi, W., Kamoun, S., Ayedi, H., and Guidara, F.K. (2012) Crystal structure, ionic conductivity and dielectric relaxation studies in the $(C_5H_{10}N)_2BiBr_5$ compound. **Physica B**, 407, p. 2365.

Medycki, W., Holderna-Natkaniec, K., Swiergiel, J., and Jakubas, R. (2003) Molecular dynamics in ferroelectric 4-aminopyridinium tetrachloroantimonate (III), [4-$NH_2C_5H_4$ NH][$SbCl_4$]. **Solid State Nucl. Magn. Reson.**, 24, p. 209.

Milankovic, A.M., Santic, A., Licina, V., and Day, D.E. (2005) Dielectric behavior and impedance spectroscopy of bismuth iron phosphate glasses. **J. Non-Cryst. Solids**, 351, p. 3235.

Nithya, H., Selvasekarapandian, S., Kumar, D.A., Sakunthala, A., Hema, M., Christopherselvin, P., Kawamura, J., and Sanjeeviraja, R.B. (2011) Thermal and dielectric studies of polymer electrolyte based on P(ECH-EO). **Mater. Chem. Phys. C**, 126, p. 404.

Padmasree, K.P., and Kanchan, D.K. (2005) Modulus studies of CdI_2–Ag_2O–V_2O_5–B_2O_3 system. **Mater. Sci. Eng:, B**, 122, pp. 24-28.

Prabakar, K., Narayandass, S.K., and Mangalaraj, D. (2003) Dielectric studies on $Cd_{0.4}Zn_{0.6}Te$ thin films. **Materials Chemistry and Physics**, 78, p. 809.

Rao, K.S., Prasad, D.M., Krishna, P.M., and Lee, J.H. (2008) Synthesis, electrical and electromechanical properties of a tungsten-bronze ceramic oxide: $Pb_{0.68}K_{0.64}Nb_2O_6$. **Physica B**, 403, p. 2079.

Rhouma, F.I., Dhahri, H.A., Dhahri, J., Belmabrouk, H., and Valente, M.A. (2012) Structural and dielectric properties of $Ba_{0.8}La_{0.133}Ti_{0.90}Sn_{0.1}O_3$. **Solid State Commun.**, 152, p. 1874.

Weslati, N., Chaabane, I., and Hlel, F. (2014) A theoretical study on the molecular structure and vibrational (FT-IR and Raman) spectra of a new organic–inorganic compound of 2[$N(C_3H_7)_4$]$SbCl_4$. **Vib. Spectrosc.**, 73, p. 116.

Weslati, N., Chaabane, I., Bulou, A., and Hlel, F. (2014) Synthesis, crystal structure, thermal and dielectric properties of tetrapropylammonium tetrachloroantimonate (III). **Physica B: Condensed Matter**, 441, p. 42.

Wojtas, M., Jakubas, R., Zaleski, J., Bator, G., and Baran, J. (2008) The phase situation and ferroelectric properties in the mixed crystals [4-NH_2PyH] [$SbCl_{4(1-x)}Br_{4x}$]. **J. Mol. Struct.**, 887, p. 262.